Spot-On: robust model-based analysis of single-particle tracking experiments

Anders S Hansen[1,2,6], Maxime Woringer[1,3,4,6], Jonathan B Grimm[5], Luke D Lavis[5], Robert Tjian[1,2], Xavier Darzacq[1]

[1]Department of Molecular and Cell Biology, Li Ka Shing Center for Biomedical and Health Sciences, CIRM Center of Excellence, University of California, Berkeley, CA 94720, USA.
[2]Howard Hughes Medical Institute, Berkeley, CA 94720, USA
[3]Unité Imagerie et Modélisation, Institut Pasteur, 25 rue du Docteur Roux, 75015 Paris, France
[4]Sorbonne Universités, UPMC Univ Paris 06, IFD, 4 Place Jussieu, 75252 Paris cedex 05, France
[5]Janelia Research Campus, Howard Hughes Medical Institute, Ashburn, VA, USA
[6]These authors contributed equally and are alphabetically listed.

*Correspondence to: anders.sejr.hansen@berkeley.edu (ASH); jmlim@berkeley.edu (RT); darzacq@berkeley.edu (XD)

Abstract

Single-particle tracking (SPT) has become a popular method for studying intracellular protein dynamics in live cells, but easy-to-use analysis tools are lacking. Here, we introduce "Spot-On", an online kinetic modeling framework that accounts for known biases and robustly infers diffusion constants and subpopulations from pooled single-molecule trajectories. We validate Spot-On using experimentally realistic simulations and then apply Spot-On to SPT data from live mammalian cells spanning a wide range of nuclear dynamics.

Main text

Recent advances in imaging technologies, genetically encoded tags and fluorophore development have made single-particle tracking (SPT) an increasingly popular method for analyzing protein dynamics[1]. Compared with indirect and bulk techniques such as Fluorescence Recovery After Photobleaching (FRAP) or Fluorescence Correlation Spectroscopy (FCS), SPT is often seen as less biased and less model-dependent[2]. In particular, SPT makes it possible to directly follow single molecules over time in live cells and has provided clear evidence that proteins often exist in several subpopulations that can be characterized by their distinct diffusion coefficients[2]. Transcription factors (TFs), for example, typically show a quasi-immobile chromatin-bound fraction and a freely diffusing fraction inside the nucleus. However, while SPT of slow-diffusing membrane proteins is an established technology, 2D-SPT of proteins freely diffusing inside a 3D nucleus introduces several biases, which must be corrected for in order to obtain accurate estimates of subpopulations. First, while a frame is acquired, fast-diffusing molecules move and spread out their emitted photons over multiple pixels causing a "*motion-blur*" artifact[3,4], whereas immobile or slow-diffusing molecules resemble point spread functions (PSFs; Fig. 1a). This results in under-counting of the fast-diffusing subpopulation. Second, high particle densities tend to cause *tracking errors* when localized molecules are connected into trajectories. This can result in incorrect displacement estimates (Fig. 1b). Third, since SPT generally employs 2D imaging of 3D motion, immobile or slow-diffusing molecules will generally remain in-focus until they photobleach and therefore exhibit long trajectories, whereas fast-diffusing molecules in 3D rapidly move out-of-focus, thus resulting in short trajectories ("*defocalization*"; Fig. 1c). This results in a time-dependent under-counting of fast-diffusing molecules[5]. Fourth, SPT *analysis methods* themselves may introduce biases; to avoid this an unbiased method

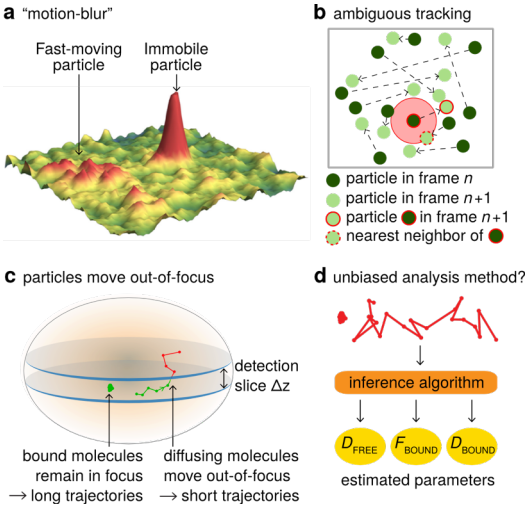

Figure 1. Bias in single-particle tracking (SPT) experiments and analysis methods. (**a**) "Motion-blur" bias. Constant excitation during acquisition of a frame will cause a fast-moving particle to spread out its emission photons over many pixels and thus appear as a motion-blur, which make detection much less likely with common PSF-fitting algorithms. In contrast, a slow-moving or immobile particle will appear as a well-shaped PSF and thus readily be detected. (**b**) Tracking ambiguities. Tracking at high particle densities prevents unambiguous connection of particles between frames and tracking errors will cause displacements to be misidentified. (**c**) Defocalization bias. During 2D-SPT, fast-moving particles will rapidly move out-of-focus resulting in short trajectories, whereas immobile particles will remain in-focus until they photobleach and thus exhibit very long trajectories. This results in a bias toward slow-moving particles, which must be corrected for. (**d**) Analysis method. Any analysis method should ideally avoid introducing biases and accurately correct for known biases in the estimation of subpopulation parameters such as D_{FREE}, F_{BOUND}, D_{BOUND}.

is needed (Fig. 1d). The first two biases must be minimized at the data acquisition stage and we describe a method to do so below (spaSPT), whereas the latter two can be overcome using a previously developed kinetic modeling framework[6,7] now extended and implemented in Spot-On. Spot-On is available as a web-interface (https://SpotOn.berkeley.edu) as well as Python and Matlab packages.

Spot-On is a user-friendly web-interface that pedagogically guides the user through a series of quality-checks of uploaded datasets consisting of pooled single-molecule trajectories. It then performs kinetic model-based analysis that leverages the histogram of molecular displacements over time to infer the fraction and diffusion constant of each subpopulation (Fig 2a). Crucially, not only does Spot-On correct defocalization bias (Fig. 1c) by compensating using the probability of each subpopulation moving out-of-focus as a function of time, it also uses the loss of fast-diffusing molecules over time as additional information to infer the diffusion constant and size of each subpopulation.

To use Spot-On, a user uploads their SPT trajectory data in one of several formats (Fig. 2a). Spot-On then generates useful meta-data for assessing the quality of the experiment (e.g. localization density, number of trajectories etc.). Spot-On also allows a user to upload multiple datasets (e.g. different replicates) and merge them. Spot-On then calculates and displays

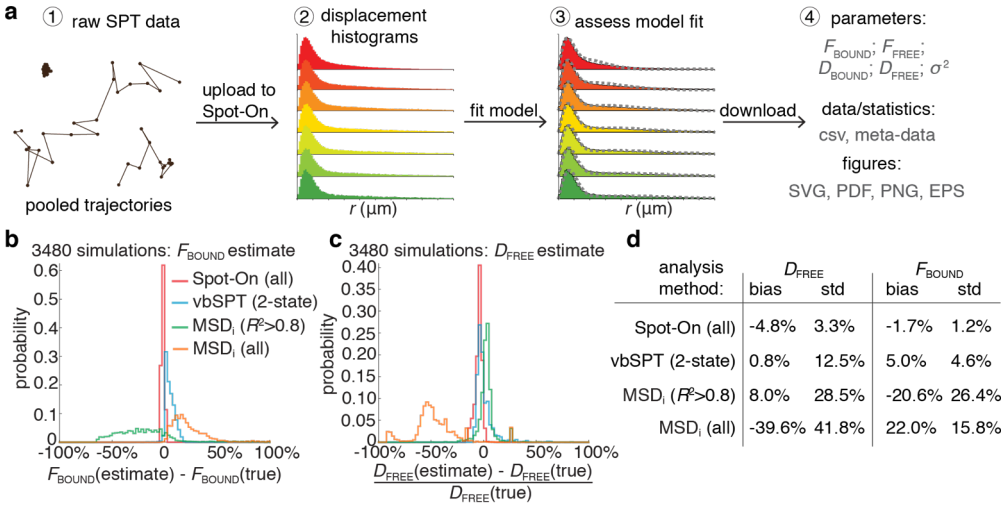

analysis method:	D_{FREE} bias	D_{FREE} std	F_{BOUND} bias	F_{BOUND} std
Spot-On (all)	-4.8%	3.3%	-1.7%	1.2%
vbSPT (2-state)	0.8%	12.5%	5.0%	4.6%
MSD$_i$ (R^2>0.8)	8.0%	28.5%	-20.6%	26.4%
MSD$_i$ (all)	-39.6%	41.8%	22.0%	15.8%

Figure 2. Overview of Spot-On and simulation results. (**a**) Overview of Spot-On. To use Spot-On, a user uploads raw SPT data in the form of pooled SPT trajectories to the Spot-On webinterface. Spot-On then calculates displacement histograms. The user inputs relevant experimental descriptors and chooses a model to fit. After model-fitting, the user can then download model-inferred parameters, meta-data and download publication-quality figures. (**b-c**) Simulation results. Experimentally realistic SPT data was simulated inside a spherical mammalian nucleus with a radius of 4 μm subject to highly-inclined and laminated optical sheet illumination[9] (HiLo) of thickness 4 μm illuminating the center of the nucleus. The axial detection window was 700 nm with Gaussian edges and particles were subject to a 25 nm localization error in all three dimensions. Photobleaching corresponded to a mean trajectory length of 4 frames inside the HiLo sheet and 40 outside. 3480 experiments were simulated with parameters of D_{FREE}=[0.5;14.5] in steps of 0.5 μm^2/s and F_{BOUND}=[0;95% in steps of 5% and the frame rate correspond to $\Delta\tau$=[1,4,7,10,13,20] ms. Each experiment was then fitted using Spot-On, using vbSPT (maximum of 2 states allowed)[8], MSD$_i$ using all trajectories of at least 5 frames (MSD$_i$ (all)) or MSD$_i$ using all trajectories of at least 5 frames where the MSD-curvefit showed at least R^2>0.8 (MSD$_i$ (R^2>0.8)). (**b**) shows the distribution of absolute errors in the F_{BOUND}–estimate and (**c**) shows the distribution of relative errors in the D_{FREE}–estimate. (**d**) Summary of simulation results. The table shows the bias (mean error) and the standard deviation (std) for each method for all 3480 simulations. The left column shows the relative bias/std for the D_{FREE}-estimate and the right column shows the absolute bias/std for the F_{BOUND}-estimate.

histograms of displacements over multiple time delays. The next step is model fitting. Spot-On models the distribution of displacements for each subpopulation using Brownian motion under steady-state conditions, while accounting for localization errors (either user-defined or inferred from the data). Spot-On considers either 2 or 3 subpopulations. For instance, TFs in nuclei can generally exist in both a chromatin-bound state characterized by slow diffusion and a freely diffusing state associated with rapid diffusion. In this case, a 2-state model is generally appropriate ("bound" vs. "free"). Spot-On allows a user to choose their desired model and parameter ranges and then fits the model to the data. Using the previous example of TF dynamics, this allows the user to infer the bound fraction and the diffusion constants. Finally, once a user has finished fitting an appropriate model to their data, Spot-On allows easy download of publication-quality figures and relevant data (Fig. 2a).

We first evaluated whether Spot-On could robustly infer subpopulations (Fig. 1d) and successfully account for known biases (Fig. 1c) using simulated data. We also compared Spot-On to a popular alternative approach of first fitting the mean square displacement (MSD) of individual trajectories and then fitting the distribution of estimated diffusion constants ("MSD_i approach") as well as a Hidden-Markov Model-based inference method (vbSPT)[8]. Since most SPT data is collected using highly inclined illumination[9] (HiLo), we simulated TF binding and diffusion dynamics confined inside a mammalian nucleus under realistic HiLo SPT experimental settings and considered 3480 different conditions that span the full range of biologically plausible dynamics (Supplementary Fig. 1-6; Supplementary Note 1-2). Spot-On robustly inferred subpopulation sizes with minimal error (Fig. 2b-d), but slightly underestimated the diffusion constant (-4.8%; Fig. 2c-d; Supplementary Fig. 1-2). However, this underestimate was due to particle confinement inside the nucleus: Spot-On correctly inferred the diffusion constant when the confinement was relaxed (Supplementary Fig. 3). This emphasizes that diffusion constants measured by SPT inside cells should be viewed as apparent diffusion constants. In contrast, the MSD_i method failed under most conditions regardless of whether all trajectories were used (MSD_i (all)) or a fitting filter applied (MSD_i (R^2>0.8); Fig. 2b-d; Supplementary Fig. 1-2). vbSPT performed almost as well as Spot-On for slow-diffusing proteins, but showed larger deviations for fast-diffusing proteins (Supplementary Fig. 1-2) likely because vbSPT does not correct for defocalization bias. Taken together, the simulations suggest that Spot-On successfully overcomes defocalization and analysis method biases (Fig. 1c-d) and accurately estimates subpopulations and diffusion constants across a wide range of dynamics.

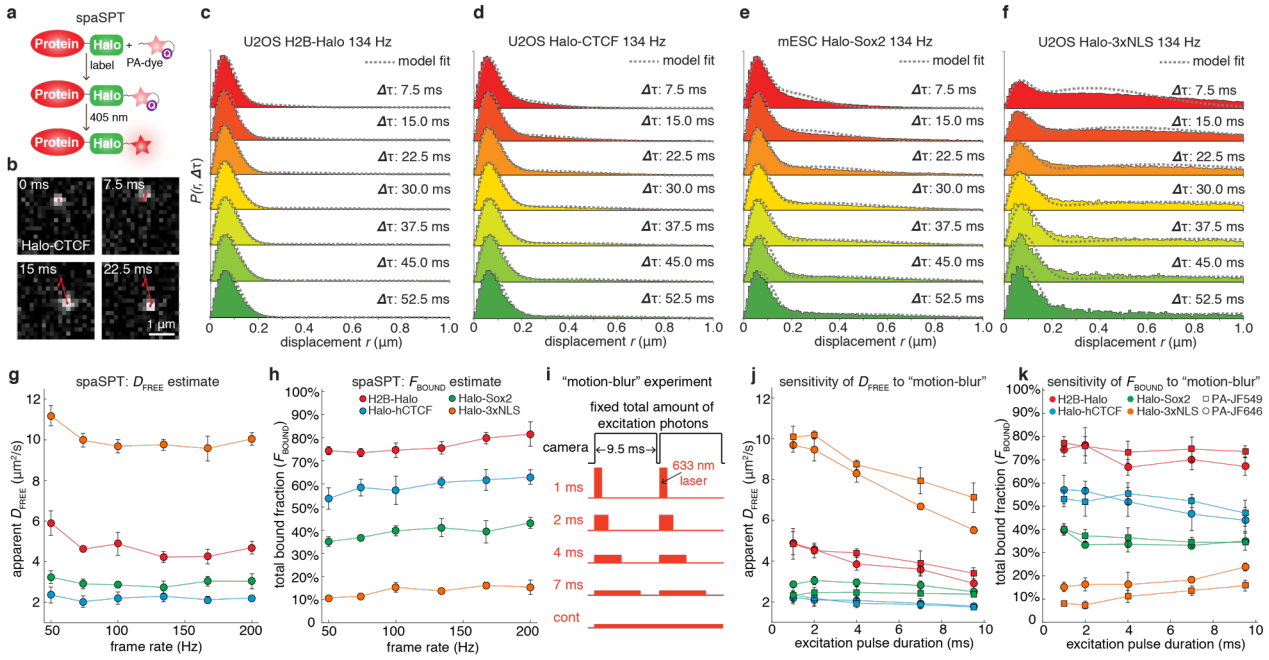

Figure 3. Overview of spaSPT and experimental results. (**a**) spaSPT. HaloTag-labeling with UV (405 nm) photo-activatable dyes enable spaSPT. spaSPT minimizes tracking errors through photo-activation which maintains low densities. (**b**) Example data. Raw spaSPT images for Halo-CTCF tracked in human U2OS cells at 134 Hz. (**c-f**) Histograms of displacements for multiple **Δτ** of histone H2B-Halo in U2OS cells (**c**), Halo-CTCF in U2OS cells (**d**), Halo-Sox2 in mES cells (**e**) and Halo-3xNLS in U2OS cells (**f**). (**g-h**) Effect of frame-rate on D_{FREE} and F_{BOUND}. spaSPT was performed at 200 Hz, 167 Hz, 134 Hz, 100 Hz, 74 Hz and 50 Hz using the 4 cell lines and the data fit using Spot-On and a 2-state model. Each experiment on each cell line was performed in 4 replicates on different days and ~5 cells imaged each day. Error bars show standard deviation between replicates. (**i**) Motion-blur experiment. To investigate the effect of "motion-blurring", the total number of excitation photons was kept constant, but delivered during pulses of duration 1, 2, 4, 7 ms or continuous (cont) illumination. (**j-k**) Effect of motion-blurring on D_{FREE} and F_{BOUND}. spaSPT data was recorded at 100Hz and 2-state model-fitting performed with Spot-On. The inferred D_{FREE} (**j**) and F_{BOUND} (**k**) were plotted as a function of excitation pulse duration. Each experiment on each cell line was performed in 4 replicates on different days and ~5 cells imaged each day. Error bars show standard deviation between replicates.

We next sought to evaluate Spot-On on experimental data. To generate SPT data with minimal acquisition bias we performed stroboscopic photo-activation SPT (spaSPT; Fig. 3a). First, spaSPT minimizes motion-blurring (Fig. 1a) by using stroboscopic excitation[10]. We found that the bright and photo-stable dyes PA-JF549 and PA-JF646[11] made it possible to achieve a signal-to-background ratio greater than 5 with just 1 ms excitation pulses, thus providing a good compromise between minimal motion-blurring and high signal (Fig. 3b). Second, spaSPT minimizes tracking errors (Fig. 1b) by using photo-activation (Fig. 3a)[11,12]. This allows tracking at extremely low densities (<1 molecule per nucleus per frame) and thereby minimizes tracking errors[4], whilst at the same time generating thousands of trajectories. To consider the full spectrum of nuclear protein dynamics, we studied histone H2B-Halo (overwhelmingly bound; fast diffusion; Fig. 3c), Halo-CTCF[7] (largely bound; very slow diffusion; Fig. 3d) and Halo-NLS (overwhelmingly free; very fast diffusion; Fig. 3f) in human U2OS cells and Halo-Sox2[13] (largely free; slow diffusion; Fig. 3e) in mouse embryonic stem cells (mESCs). We labeled Halo-tagged proteins in live cells with PA-JF549 or PA-JF646[11] and performed spaSPT using HiLo illumination. To generate a large dataset to comprehensively test Spot-On, we performed over 1064 spaSPT experiments across 60 different conditions.

First, we studied whether Spot-On could consistently infer subpopulations over a wide range of frame rates. Accordingly, we performed spaSPT at 200 Hz, 167 Hz, 134 Hz, 100 Hz, 74 Hz and 50 Hz using the four cell lines. Spot-On consistently inferred the diffusion constant (Fig. 3g) and total bound fraction across the wide range of frame rates (Fig. 3h). This is notable since all four proteins exhibit apparent anomalous diffusion (Supplementary Fig. 7). These results provide additional validation for the bias corrections implemented in Spot-On. We then sub-sampled the data sets and found that just ~3000 short trajectories were sufficient for Spot-On to reliably infer the underlying dynamics (Supplementary Fig. 8). Thus, this now makes it possible to study cell-to-cell variability in TF dynamics.

Having validated Spot-On on experimental SPT data, we next applied Spot-On to estimate the effect of motion-blurring on the estimation of subpopulations. As mentioned, since most localization algorithms[14,15] achieve super-resolution through PSF-fitting, this may cause motion-blurred molecules to be undersampled, resulting in a bias towards slow-moving molecules (Fig. 1a). We estimated the extent of the bias by imaging the four cell lines at 100 Hz and keeping the total number of excitation photons constant, but varying the excitation pulse duration (1 ms, 2 ms, 4 ms, 7 ms, constant; Fig 3i). For generality, we performed these experiments using both PA-JF549 and PA-JF646 dyes[11]. We used Spot-On to fit the data and plotted the apparent free diffusion constant (Fig. 3j) and apparent total bound fraction (Fig. 3k) as a function of the excitation pulse duration. For fast-diffusing proteins like Halo-3xNLS and H2B-Halo, motion-blurring resulted in a large underestimate of the free diffusion constant, whereas the effect on slower proteins like CTCF and Sox2 was minor (Fig. 3j). Regarding the total bound fraction, motion-blurring caused a ~2-fold overestimate for rapidly diffusing Halo-3xNLS (Fig. 3k), but had a minor effect on slower proteins like H2B, CTCF and Sox2. Importantly, similar results were obtained for both dyes (Fig. 3j-k). Taken together, these results suggest that Spot-On can reliably be used even for SPT data collected under constant illumination provided that protein diffusion is sufficiently slow and, moreover, provides a helpful guide for optimizing SPT imaging acquisitions (full discussion in Supplementary Note 3).

In summary, SPT is an increasingly popular technique and has been revealing important new biological insight. Several methods are available for localization/tracking[14,15] and for classification of individual trajectories[8,16]. Spot-On now complements these tools by providing a bias-corrected, comprehensive open-source framework for inferring subpopulations and diffusion constants from pooled SPT data. This platform can easily be extended to other

169 diffusion regimes. Moreover, spaSPT provides an acquisition protocol for tracking fast-diffusing
170 molecules with minimal bias. We hope that these validated tools will help make SPT more
171 accessible to the community and contribute positively to the emergence of "gold-standard"
172 acquisition and analysis procedures for SPT.
173

Acknowledgements

We are very grateful to Davide Mazza who inspired this work and provided invaluable comments on Spot-On, to Florian Mueller for suggestions on the web-application, Christophe Zimmer for insightful discussions, David McSwiggen and Sheila Teves for kindly providing cell lines, Carolyn Elya and Chiahao Tsui for the name "Spot-On", and to members of the Tjian/Darzacq labs for discussions. We also thank Astou Tangara and Anatalia Robles for microscope maintenance. ASH is a postdoctoral fellow of the Siebel Stem Cell Institute. This work was supported by NIH grants UO1-EB021236 and U54-DK107980 (XD), the California Institute of Regenerative Medicine grant LA1-08013 (XD), and by the Howard Hughes Medical Institute (003061, RT).

Author contributions

ASH, MW and XD conceived the project. ASH and MW developed Spot-On, performed simulations, analyzed experiments and drafted the manuscript. ASH performed experiments. JBG and LDL developed and contributed JF dyes. RT and XD supervised the project. All authors edited the manuscript. ASH and MW contributed equally and are listed in alphabetical order on the first page.

Competing financial interests

JBG and LDL declare competing financial interests. The other authors declare no competing financial interests.

References

1. Liu, Z., Lavis, L. D. & Betzig, E. Imaging Live-Cell Dynamics and Structure at the Single-Molecule Level. *Molecular Cell* **58,** 644 (2015).
2. Shen, H. *et al*. Single Particle Tracking: From Theory to Biophysical Applications. *Chem. Rev*. **117,** 7331–7376 (2017).
3. Berglund, A. J. Statistics of camera-based single-particle tracking. *Phys. Rev. E - Stat. Nonlinear, Soft Matter Phys*. **82,** (2010).
4. Izeddin, I. *et al*. Single-molecule tracking in live cells reveals distinct target-search strategies of transcription factors in the nucleus. *Elife* **2014,** 1–27 (2014).
5. Kues, T. & Kubitscheck, U. Single molecule motion perpendicular to the focal plane of a microscope: Application to splicing factor dynamics within the cell nucleus. *Single Mol*. **3,** 218–224 (2002).
6. Mazza, D., Abernathy, A., Golob, N., Morisaki, T. & McNally, J. G. A benchmark for chromatin binding measurements in live cells. *Nucleic Acids Res*. **40,** (2012).
7. Hansen, A. S., Pustova, I., Cattoglio, C., Tjian, R. & Darzacq, X. CTCF and cohesin regulate chromatin loop stability with distinct dynamics. *Elife* **6,** (2017).
8. Persson, F., Lindén, M., Unoson, C. & Elf, J. Extracting intracellular diffusive states and transition rates from single-molecule tracking data. *Nat. Methods* **10,** 265–9 (2013).
9. Tokunaga, M., Imamoto, N. & Sakata-Sogawa, K. Highly inclined thin illumination enables clear single-molecule imaging in cells. *Nat. Methods* **5,** 159–61 (2008).
10. Elf, J., Li, G.-W. & Xie, X. S. Probing transcription factor dynamics at the single-molecule level in a living cell. *Science* **316,** 1191–4 (2007).
11. Grimm, J. B. *et al*. Bright photoactivatable fluorophores for single-molecule imaging. *Nat. Methods* 66779 (2016). doi:10.1101/066779
12. Manley, S. *et al*. High-density mapping of single-molecule trajectories with photoactivated localization microscopy. *Nat. Methods* **5,** 155–157 (2008).
13. Teves, S. S. *et al*. A dynamic mode of mitotic bookmarking by transcription factors. *Elife* **5,** (2016).
14. Chenouard, N. *et al*. Objective comparison of particle tracking methods. *Nat Meth* **11,** 281–289 (2014).
15. Sergé, A., Bertaux, N., Rigneault, H. & Marguet, D. Dynamic multiple-target tracing to probe spatiotemporal cartography of cell membranes. *Nat. Methods* **5,** 687–694 (2008).
16. Monnier, N. *et al*. Inferring transient particle transport dynamics in live cells. *Nat Meth* **12,** 838–840 (2015).
17. Matsuoka, S., Shibata, T. & Ueda, M. Statistical analysis of lateral diffusion and multistate kinetics in single-molecule imaging. *Biophys. J*. **97,** 1115–1124 (2009).

18. Carslow, H. S. & Jaeger, J. C. *Conduction of Heat in Solids*. *Oxford University Press* (1959).
19. Pettitt, S. J. *et al*. Agouti C57BL/6N embryonic stem cells for mouse genetic resources. *Nat*. *Methods* **6,** 493–5 (2009).

MATERIALS AND METHODS

Spot-On model. Spot-On implements and extends a kinetic modeling framework first described in Mazza *et al.*[6] and later extended in Hansen *et al.*[7] The evolution over time of a concentration of particles located at the origin as a Dirac delta function and which follows free diffusion in two dimensions with a diffusion constant D can be described by a propagator (also known as Green's function). Properly normalized, the probability of a particle starting at the origin ending up at a location $r = (x,y)$ after a time delay, $\Delta\tau$, is given by:

$$P(r,\Delta\tau) = N\frac{r}{2D\Delta\tau}e^{-\frac{r^2}{4D\Delta\tau}}$$

Here N is a normalization constant with units of length. Spot-On integrates this distribution over a small histogram bin window, Δr, to obtain a normalized distribution to compare to binned experimental data. For simplicity, we will therefore leave out N from subsequent expressions. Since experimental SPT data is subject to a significant localization error, σ, Spot-On also accounts for this[17]:

$$P(r,\Delta\tau) = \frac{r}{2(D\Delta\tau+\sigma^2)}e^{-\frac{r^2}{4(D\Delta\tau+\sigma^2)}}$$

Many proteins studied by SPT can generally exist in a quasi-immobile state (e.g. a chromatin-bound state in the case of transcription factors) and one or more mobile states. We will first consider the 2-state model. Under most conditions, state transitions can be ignored[7]. Thus, the steady-state 2-state model considered by Spot-On becomes:

$$P(r,\Delta\tau) = F_{\mathrm{BOUND}}\frac{r}{2(D_{\mathrm{BOUND}}\Delta\tau+\sigma^2)}e^{-\frac{r^2}{4(D_{\mathrm{BOUND}}\Delta\tau+\sigma^2)}} + (1-F_{\mathrm{BOUND}})\frac{r}{2(D_{\mathrm{FREE}}\Delta\tau+\sigma^2)}e^{-\frac{r^2}{4(D_{\mathrm{FREE}}\Delta\tau+\sigma^2)}}$$

Here, the quasi-immobile subpopulation has diffusion constant, D_{BOUND}, and makes up a fraction, F_{BOUND}, whereas the freely diffusing subpopulation has diffusion constant, D_{FREE}, and makes up a fraction, $F_{\mathrm{FREE}} = 1 - F_{\mathrm{BOUND}}$. To account for defocalization bias (Fig. 1c), Spot-On explicitly considers the probability of the freely diffusing subpopulation moving out of the axial detection range, Δz, during each time delay, $\Delta\tau$. This is important. For example, only ~25% of freely-diffusing molecules will remain in focus for at least 5 frames (assuming $\Delta\tau$=10 ms; Δz=700 nm; 1 gap allowed; D=5 μm^2/s), resulting in a 4-fold undercounting if uncorrected for. If we assume absorbing boundaries such that any molecule that contacts the edges of the axial detection range located at $z_{\mathrm{MAX}} = \Delta z/2$ and $z_{\mathrm{MIN}} = -\Delta z/2$ is permanently lost, the fraction of freely diffusing molecules with diffusion constant, D_{FREE}, that remain at time delay, $\Delta\tau$, is given by[5,18]:

$$P_{\mathrm{remaining}}(\Delta\tau,\Delta z,D_{\mathrm{FREE}}) = \frac{1}{\Delta z}\int_{-\Delta z/2}^{\Delta z/2}\left\{1-\sum_{n=0}^{\infty}(-1)^n\left[\mathrm{erfc}\left(\frac{\frac{(2n+1)\Delta z}{2}-z}{\sqrt{4D_{\mathrm{FREE}}\Delta\tau}}\right)+\mathrm{erfc}\left(\frac{\frac{(2n+1)\Delta z}{2}+z}{\sqrt{4D_{\mathrm{FREE}}\Delta\tau}}\right)\right]\right\}\mathrm{d}z$$

However, this analytical expression overestimates the fraction lost since there is a significant probability that a molecule that briefly contacted or exceeded the boundary re-enters the axial detection range. The re-entry probability depends on the number of gaps allowed in the tracking (g), $\Delta\tau$, and Δz and can be approximately accounted for by considering a corrected axial detection range, Δz_{corr}, larger than Δz: $\Delta z_{\mathrm{corr}} > \Delta z$:

$$\Delta z_{\mathrm{corr}}(\Delta z,\Delta\tau,D_{\mathrm{FREE}},g) = \Delta z + a(\Delta z,\Delta\tau,g)\sqrt{D_{\mathrm{FREE}}} + b(\Delta z,\Delta\tau,g)$$

Although Δz_{corr} depend on the number of gaps (g) allowed in the tracking, we will leave it out for simplicity in the following. We determined the coefficients a and b from Monte Carlo simulations. For a given diffusion constant, D, 50,000 molecules were uniformly placed one-dimensionally along the z-axis from $z_{\mathrm{MIN}} = -\Delta z/2$ to $z_{\mathrm{MAX}} = \Delta z/2$. Next, using a time-step $\Delta\tau$,

one-dimensional Brownian diffusion was simulated along the z-axis using the Euler-Maruyama scheme. For time delays from $1\Delta\tau$ to $15\Delta\tau$, the fraction of molecules that were lost was calculated in the range of D=[1;12] μm^2/s. $a(\Delta z, \Delta\tau, g)$ and $b(\Delta z, \Delta\tau, g)$ were then estimated through least-squares fitting of $P_{\text{remaining}}(\Delta\tau, \Delta z_{\text{corr}}, D)$ to the simulated fraction remaining. The process was repeated over a grid of plausible values of $(\Delta z, \Delta\tau, g)$ to derive a grid of 134,865 (a,b) parameter pairs. This pre-calculated library of (a,b) parameters enables Spot-On to perform model fitting on nearly any SPT dataset with minimal overhead.

Thus, the 2-state model Spot-On uses for kinetic modeling of SPT data is given by:

$$P_2(r,\Delta\tau) = F_{\text{BOUND}} \frac{r}{2(D_{\text{BOUND}}\Delta\tau + \sigma^2)} e^{-\frac{r^2}{4(D_{\text{BOUND}}\Delta\tau+\sigma^2)}} + Z_{\text{CORR}}(\Delta\tau, \Delta z_{\text{corr}}, D_{\text{FREE}})(1 - F_{\text{BOUND}}) \frac{r}{2(D_{\text{FREE}}\Delta\tau + \sigma^2)} e^{-\frac{r^2}{4(D_{\text{FREE}}\Delta\tau+\sigma^2)}}$$

where:

$$Z_{\text{CORR}}(\Delta\tau, \Delta z_{\text{corr}}, D_{\text{FREE}}) = \frac{1}{\Delta z_{\text{corr}}} \int_{-\frac{\Delta z_{\text{corr}}}{2}}^{\frac{\Delta z_{\text{corr}}}{2}} \left\{ 1 - \sum_{n=0}^{\infty} (-1)^n \left[\text{erfc}\left(\frac{\frac{(2n+1)\Delta z_{\text{corr}}}{2} - z}{\sqrt{4D_{\text{FREE}}\Delta\tau}} \right) + \text{erfc}\left(\frac{\frac{(2n+1)\Delta z_{\text{corr}}}{2} + z}{\sqrt{4D_{\text{FREE}}\Delta\tau}} \right) \right] \right\} \mathrm{d}z$$

Having derived the 2-state model, generalization to a 3-state model with 1 bound and 2 diffusive states is straightforward. If the three subpopulations have diffusion constants D_{BOUND}, D_{SLOW}, D_{FAST}, and fractions F_{BOUND}, F_{SLOW}, F_{FAST}, such that $F_{\text{BOUND}} + F_{\text{SLOW}} + F_{\text{FAST}}$=1, then the 3-state model considered by Spot-On becomes:

$$P_3(r,\Delta\tau) = F_{\text{BOUND}} \frac{r}{2(D_{\text{BOUND}}\Delta\tau + \sigma^2)} e^{-\frac{r^2}{4(D_{\text{BOUND}}\Delta\tau+\sigma^2)}} + Z_{\text{CORR}}(\Delta\tau, \Delta z_{\text{corr}}, D_{\text{SLOW}}) F_{\text{SLOW}} \frac{r}{2(D_{\text{SLOW}}\Delta\tau + \sigma^2)} e^{-\frac{r^2}{4(D_{\text{SLOW}}\Delta\tau+\sigma^2)}} + Z_{\text{CORR}}(\Delta\tau, \Delta z_{\text{corr}}, D_{\text{FAST}})(1 - F_{\text{BOUND}} - F_{\text{SLOW}}) \frac{r}{2(D_{\text{FAST}}\Delta\tau + \sigma^2)} e^{-\frac{r^2}{4(D_{\text{FAST}}\Delta\tau+\sigma^2)}}$$

Where $Z_{\text{CORR}}(\Delta\tau, \Delta z_{\text{corr}}, D)$ is as described above.

Numerical implementation of models in Spot-On. Spot-On calculates the empirical histogram of displacements based on a user-defined bin width. Spot-On allows the user to choose between PDF- and CDF-fitting of the kinetic model to the empirical displacement distributions; CDF-fitting is generally most accurate for smaller datasets and the two are similar for large datasets (Supplementary Fig. 6). The integral in $Z_{\text{CORR}}(\Delta\tau, \Delta z_{\text{corr}})$ was numerically evaluated using the midpoint method over 200 points and the terms of the series computed until the term falls below a threshold of 10^{-10}. Model fitting and parameter optimization was performed using a non-linear least squares algorithm (Levenberg-Marquardt). Random initial parameter guesses are drawn uniformly from the user-specified parameter range. The optimization is then repeated several times with different initialization parameters to avoid local minima. Spot-On constrains each fraction to be between 0 and 1 and for the sum of the fractions to equal 1.

Cell Culture. Halo-Sox2[13] knock-in JM8.N4 mouse embryonic stem cells[19] were grown on plates pre-coated with a 0.1% autoclaved gelatin solution (Sigma-Aldrich, G9391) under feeder free conditions in knock-out DMEM with 15% FBS and LIF (full recipe: 500 mL knockout DMEM (ThermoFisher #10829018), 6 mL MEM NEAA (ThermoFisher #11140050), 6 mL GlutaMax (ThermoFisher #35050061), 5 mL Penicillin-streptomycin (ThermoFisher #15140122), 4.6 μL 2-mercapoethanol (Sigma-Aldrich M3148), 90 mL fetal bovine serum (HyClone FBS SH30910.03 lot #AXJ47554)) and LIF. mES cells were fed by replacing half the medium with fresh medium daily and passaged every two days by trypsinization. Halo-3xNLS,

315 H2B-Halo-SNAP and knock-in C32 Halo-CTCF[7] Human U2OS osteosarcoma cells were grown
316 in low glucose DMEM with 10% FBS (full recipe: 500 mL DMEM (ThermoFisher #10567014),
317 50 mL fetal bovine serum (HyClone FBS SH30910.03 lot #AXJ47554) and 5 mL Penicillin-
318 streptomycin (ThermoFisher #15140122)) and were passaged every 2-4 days before reaching
319 confluency. For live-cell imaging, the medium was identical except DMEM without phenol red
320 was used (ThermoFisher #31053028). Both mouse ES and human U2OS cells were grown in a
321 Sanyo copper alloy IncuSafe humidified incubator (MCO-18AIC(UV)) at 37°C/5.5% CO_2. Cell
322 lines were pathogen tested and authenticated through STR profiling (U2OS) as described
323 previously[7,13].
324
325 **Single-molecule imaging**. The indicated cell line was grown overnight on plasma-cleaned 25
326 mm circular no 1.5H cover glasses (Marienfeld High-Precision 0117650) either directly (U2OS)
327 or MatriGel coated (mESCs; Fisher Scientific #08-774-552 according to manufacturer's
328 instructions just prior to cell plating). After overnight growth, cells were labeled with 5-50 nM
329 PA-JF549 or PA-JF646[11] for ~15-30 min and washed twice (one wash: medium removed; PBS
330 wash; replenished with fresh medium). At the end of the final wash, the medium was changed to
331 phenol red-free medium keeping all other aspects of the medium the same. Single-molecule
332 imaging was performed on a custom-built Nikon TI microscope equipped with a 100x/NA 1.49
333 oil-immersion TIRF objective (Nikon apochromat CFI Apo TIRF 100x Oil), EM-CCD camera
334 (Andor iXon Ultra 897; frame-transfer mode; vertical shift speed: 0.9 μs; -70°C), a perfect
335 focusing system to correct for axial drift and motorized laser illumination (Ti-TIRF, Nikon),
336 which allows an incident angle adjustment to achieve highly inclined and laminated optical sheet
337 illumination[9]. The incubation chamber maintained a humidified 37°C atmosphere with 5% CO_2
338 and the objective was also heated to 37°C. Excitation was achieved using the following laser
339 lines: 561 nm (1 W, Genesis Coherent) for PA-JF549; 633 nm (1 W, Genesis Coherent) for PA-
340 JF646; 405 nm (140 mW, OBIS, Coherent) for all photo-activation experiments. The excitation
341 lasers were modulated by an acousto-optic Tunable Filter (AA Opto-Electronic, AOTFnC-VIS-
342 TN) and triggered with the camera TTL exposure output signal. The laser light is coupled into
343 the microscope by an optical fiber and then reflected using a multi-band dichroic (405 nm/488
344 nm/561 nm/633 nm quad-band, Semrock) and then focused in the back focal plane of the
345 objective. Fluorescence emission light was filtered using a single band-pass filter placed in front
346 of the camera using the following filters: PA-JF549: Semrock 593/40 nm bandpass filter; PA-
347 JF646: Semrock 676/37 nm bandpass filter. The microscope, cameras, and hardware were
348 controlled through NIS-Elements software (Nikon).
349
350 **spaSPT experiments and analysis**. The spaSPT experimental settings for Fig. 3g-h were as
351 follows: 1 ms 633 nm excitation (100% AOTF) of PA-JF646 was delivered at the beginning of
352 the frame; 405 nm photo-activation pulses were delivered during the camera integration time
353 (~447 μs) to minimize background and their intensity optimized to achieve a mean density of ≤1
354 molecule per frame per nucleus. 30,000 frames were recorded per cell per experiment. The
355 camera exposure times were: 4.5 ms, 5.5 ms, 7 ms, 9.5 ms, 13 ms and 19.5 ms.
356 For the motion-blur spaSPT experiments (Fig. 3i-k), the camera exposure was fixed to 9.5 ms
357 and photo-activation performed as above. To keep the total number of delivered photons
358 constant, we generated an AOTF-laser intensity calibration curve using a power meter and
359 adjusted the AOTF transmission accordingly for each excitation pulse duration. The excitation
360 settings were as follows: 1 ms, 561 nm 100% AOTF, 633 nm 100% AOTF; 2 ms, 561 nm 43%
361 AOTF, 633 nm 40% AOTF; 4 ms, 561 nm 28% AOTF, 633 nm 27% AOTF; 7 ms, 561 nm 20%
362 AOTF, 633 nm 19% AOTF; constant illumination, 561 nm 17% AOTF, 633 nm 16% AOTF.

spaSPT data was analyzed (localization and tracking) and converted into trajectories using a custom-written Matlab implementation of the MTT-algorithm[15] and the following settings: Localization error: $10^{-6.25}$; deflation loops: 0; Blinking (frames): 1; max competitors: 3; max D ($\mu m^2/s$): 20. The spaSPT trajectory data was then analyzed using the Matlab version of Spot-On (v1.0; GitLab tag 1f9f782b) and the following parameters: dZ=0.7 μm; GapsAllowed=1; TimePoints: 4 (50 Hz), 6 (74 Hz), 7 (100 Hz), 8 (134 Hz), 9 (167 and 200 Hz); JumpsToConsider=4; ModelFit=2; NumberOfStates=2; FitLocError=0; LocError=0.035 μm; D_Free_2State=[0.4;25]; D_Bound_2State=[0.00001;0.08];

SPT simulations. We developed a utility to simulate diffusing proteins in a confined geometry (simSPT). Briefly, simSPT simulates the diffusion of an arbitrary number of populations of molecules characterized by their diffusion coefficient, under a steady state assumption. Particles are drawn at random between the populations and their location in the 3D nucleus is initialized following a uniform law within the confinement volume. The lifetime of the particle (in frames) is also drawn following an exponential law of mean lifetime β. Then, the particle diffuses in 3D until it bleaches. Diffusion is simulated by drawing jumps following a normal law of parameters $\sim N\left(0, \sqrt{2D\Delta\tau}\right)$, where D is the diffusion coefficient and $\Delta\tau$ the exposure time. Finally, a localization error ($\sim N(0, \sigma)$) is added to each (x,y,z) localization in the simulated trajectories. For this work, we parameterized simSPT to consider that two subpopulations of particles diffuse in a sphere (the nucleus) of 8 μm diameter illuminated using HiLo illumination (assuming a HiLo beam width of 4 μm), with an axial detection range of ~700 nm, centered at the middle of the HiLo beam. Molecules are assumed to have a mean lifetime of 4 frames (when inside the HiLo beam) and of 40 frames when outside the HiLo beam. The localization error was set to 25 nm and the simulation was run until 100000 in-focus trajectories were recorded. More specifically, the effect of the exposure time (1 ms, 4 ms, 7 ms, 13 ms, 20 ms), the free diffusion constant (from 0.5 $\mu m^2/s$ to 14.5 $\mu m^2/s$ in 0.5 $\mu m^2/s$ increments) and the fraction bound (from 0 % to 95 % in 5 % increments) were investigated, yielding a dataset consisting of 3480 simulations. More details on the simulations, including scripts to reproduce the dataset, are available on GitLab as detailed in the "Computer code" section. Full details on how the simulations were analyzed by Spot-On and MSD_i is given in Supplementary Note 1.

Data availability. All raw 1064 spaSPT experiments as well as the 3480 simulations (Fig. 2b-c) are freely available in Spot-On readable Matlab and CSV file formats in the form of SPT trajectories at Zenodo. After publication, experimental data will be available at Zenodo. Before publication all experimental data is available upon request; The simulations are available in Matlab format at: https://zenodo.org/record/835541; The simulations are available in CSV format at: https://zenodo.org/record/834787; And supplementary software used for MSD_i and vbSPT analysis as well as for generating the simulated data at: https://zenodo.org/record/835171

Computer code. Spot-On is fully open-source. The web-interface can be found at: https://SpotOn.berkeley.edu. All raw code is available at GitLab: https://gitlab.com/tjian-darzacq-lab. The web-interface code can be found at https://gitlab.com/tjian-darzacq-lab/Spot-On; the Matlab command-line version of Spot-On can be found at: https://gitlab.com/tjian-darzacq-lab/spot-on-matlab; the Python command-line version of Spot-On can be found at https://gitlab.com/tjian-darzacq-lab/Spot-On-cli; finally, the SPT simulation code (simSPT) can be found at: https://gitlab.com/tjian-darzacq-lab/simSPT.

Supplementary Information:

Supplementary Information includes the following notes:

- Supplementary Note 1: Fitting of simulations using Spot-On, vbSPT and MSD_i
- Supplementary Note 2: Considerations for choosing Spot-On parameters
- Supplementary Note 3: SPT acquisition considerations in spaSPT experiments

And the following Supplementary Figures:

- Supplementary Figure 1: Comparison of Spot-On, vbSPT and MSDi estimates of D_{FREE} and F_{BOUND} to ground-truth simulation results inside a 4 μm radius nucleus.
- Supplementary Figure 2. Representative fits for Spot-On, vbSPT and MSDi to ground-truth simulation results.
- Supplementary Figure 3. Comparison of Spot-On, vbSPT and MSDi estimates of D_{FREE} and F_{BOUND} to ground-truth simulation results inside a 20 μm radius nucleus. Supplementary Figure 4. Sensitivity of Spot-On to the axial detection range.
- Supplementary Figure 5. Sensitivity of Spot-On to the number of timepoints considered.
- Supplementary Figure 6. Comparison of Spot-On and MSDi estimates of D_{FREE} and F_{BOUND} to ground-truth simulation results inside a 4 μm radius nucleus using PDF-fitting.
- Supplementary Figure 7. Sensitivity of Spot-On to anomalous diffusion.
- Supplementary Figure 8. Sensitivity of Spot-On, vbSPT and MSD_i (R^2>0.8) to sample size.